Title

High-Temporal-Resolution Lung Kinetic Modeling Using Total-Body Dynamic PET with Time-Delay and Dispersion Corrections

Journal

Journal of Nuclear Medicine, 64(7)

ISSN

0161-5505

Authors

Wang, Yiran

Spencer, Benjamin A

Schmall, Jeffrey

et al.

Publication Date

2023-07-01

DOI

10.2967/jnumed.122.264810

Peer reviewed

High-Temporal-Resolution Lung Kinetic Modeling Using Total-Body Dynamic PET with Time-Delay and Dispersion Corrections

Yiran Wang[1,2], Benjamin A. Spencer[1,2], Jeffrey Schmall[3], Elizabeth Li[2], Ramsey D. Badawi[1,2], Terry Jones[1], Simon R. Cherry[1,2], and Guobao Wang[1]

[1]Department of Radiology, University of California Davis Medical Center, Sacramento, California; [2]Department of Biomedical Engineering, University of California at Davis, Davis, California; and [3]United Imaging Healthcare of America, Inc., Houston, Texas

Tracer kinetic modeling in dynamic PET has the potential to improve the diagnosis, prognosis, and research of lung diseases. The advent of total-body PET systems with much greater detection sensitivity enables high-temporal-resolution (HTR) dynamic PET imaging of the lungs. However, existing models may become insufficient for modeling the HTR data. In this paper, we investigate the necessity of additional corrections to the input function for HTR lung kinetic modeling. **Methods:** Dynamic scans with HTR frames of as short as 1 s were performed on 13 healthy subjects with a bolus injection of about 370 MBq of ^{18}F-FDG using the uEXPLORER total-body PET/CT system. Three kinetic models with and without time-delay and dispersion corrections were compared for the quality of lung time–activity curve fitting using the Akaike information criterion. The impact on quantification of ^{18}F-FDG delivery rate K_1, net influx rate K_i and fractional blood volume v_b was assessed. Parameter identifiability analysis was also performed to evaluate the reliability of kinetic quantification with respect to noise. Correlation of kinetic parameters with age was investigated. **Results:** HTR dynamic imaging clearly revealed the rapid change in tracer concentration in the lungs and blood supply (i.e., the right ventricle). The uncorrected input function led to poor time–activity curve fitting and biased quantification in HTR kinetic modeling. The fitting was improved by time-delay and dispersion corrections. The proposed model resulted in an approximately 85% decrease in K_1, an approximately 75% increase in K_i, and a more reasonable v_b (~0.14) than the uncorrected model (~0.04). The identifiability analysis showed that the proposed models had good quantification stability for K_1, K_i, and v_b. The v_b estimated by the proposed model with simultaneous time-delay and dispersion corrections correlated inversely with age, as would be expected. **Conclusion:** Corrections to the input function are important for accurate lung kinetic analysis of HTR dynamic PET data. The modeling of both delay and dispersion can improve model fitting and significantly impact quantification of K_1, K_i, and v_b.

Key Words: total-body PET; kinetic modeling; dynamic PET; lung; high temporal resolution

J Nucl Med 2023; 64:1154–1161
DOI: 10.2967/jnumed.122.264810

PET with ^{18}F-FDG or other radiotracers is a promising method for studying a variety of lung diseases, including lung cancer (*1*), acute lung injury (*2,3*), asthma (*4*), lung fibrosis (*5*), and recently coronavirus disease 2019 (*6*). The SUV is a traditional semiquantitative measure for evaluating lung ^{18}F-FDG uptake (*7,8*), whereas kinetic analysis through compartment modeling (*9*) has shown the potential to provide more quantitative tracer kinetics, for example, the ^{18}F-FDG delivery rate K_1 (*10*), net influx rate K_i (*11–15*), and fractional blood volume v_b (*13,16*), to better characterize lung diseases in previous human and animal studies. However, conventional PET scanners have a relatively poor sensitivity and limited temporal resolution (e.g., 10–40 s/frame) for dynamic imaging, which in turn affects the performance of lung kinetic quantification.

The advent of the uEXPLORER (United Imaging) total-body PET and other scanners with a long axial field of view (*17–19*) has brought new opportunities to improve lung kinetic modeling by offering a large axial field of view to cover the entire lungs with improved detection efficiency, allowing high-temporal-resolution (HTR) imaging, such as with 1 s or even a subsecond per frame (*20,21*). The HTR ability is especially useful for capturing the rapidly changing early phase of tracer uptake in lung tissues. Meanwhile, image-derived input functions (IDIFs) can also be extracted with HTR from major blood pools (e.g., ventricles and large blood vessels) for kinetic modeling (*21,22*). In this work, we investigate the use of HTR data for lung kinetic quantification with total-body PET, expecting improvement especially for those parameters that are sensitive to the early kinetics, such as ^{18}F-FDG K_1 and v_b.

One challenge with using HTR data is the potential need for additional corrections for the IDIF. Recent work on total-body PET kinetic modeling has considered time-delay correction to account for the difference between the tracer arrival time in a tissue and the arrival in the blood pool, where the IDIF is extracted (*21–23*). However, dispersion (*24,25*) may also occur when the tracer travels from the location at which the IDIF is determined to the capillaries of the lungs. The correction for either time delay or dispersion has only rarely been investigated in previous studies of lung kinetic modeling and is usually omitted (*2,26–28*), partly because of the limited temporal resolution (e.g., 10 s/frame) of conventional dynamic PET. Here, we hypothesize that a simultaneous correction for both the time-delay and dispersion effects is essential for accurate kinetic modeling in HTR dynamic PET imaging of the lungs.

MATERIALS AND METHODS

HTR Dynamic Data Acquisition on uEXPLORER

Thirteen healthy human subjects (age [mean±SD], 49 ± 15 y; weight 82 ± 18 kg; 6 men, 7 women) gave written informed consent

Received Aug. 22, 2022; revision accepted Feb. 22, 2023.
For correspondence or reprints, contact Yiran Wang (yrdwang@ucdavis.edu).
Published online Apr. 28, 2023.

and were scanned on a uEXPLORER total-body PET/CT system (*29,30*). The study was approved by the Institutional Review Board at the University of California, Davis. After an ultralow-dose CT scan (140 kVp, 5 mAs), each participant underwent a dynamic ^{18}F-FDG PET scan with intravenous bolus administration of a dose of approximately 370 MBq. Total-body PET imaging was performed for 60 min starting immediately before the injection. The resulting list-mode data were reconstructed into dynamic images using the vendor-supplied time-of-flight ordered-subset expectation maximization algorithm with 4 iterations and 20 subsets and a voxel size of $4 \times 4 \times 4$ mm^3. The dynamic framing protocol contains 120 frames over 60 min: 60×1 s, 30×2 s, 6×10 s, 6×30 s, 12×120 s, and 6×300 s, with HTR frames (1–2 s/frame) over the first 2 min. For each subject, a region of interest (ROI) was placed in the right ventricle to extract an IDIF $C_{RV}(t)$ to represent the pulmonary blood supply, the dominant blood input to the lungs (*31,32*). Five ROIs were placed in the left and right lungs (1 in each of the 5 lung lobes) to extract lung time–activity curves from the dynamic images with diminished effects of motion and spillover. The 5 lung-ROI time–activity curves were averaged to generate a global lung time–activity curve $\check{C}_T(t)$ for each of the 13 subjects. An additional ROI was also placed in the left ventricle to extract the time–activity curve $C_{LV}(t)$ for the purpose of comparison. In addition to the HTR time–activity curves, time–activity curves of low temporal resolution were generated using 10 s/frame for the first 3 min for all the ROIs.

Compartmental Modeling

^{18}F-FDG kinetics in the extravascular lung is described by a 2-tissue irreversible (2Ti) compartmental model (*33*) and is illustrated in Figure 1A. Suppose that $C_p(t)$ is the blood input function and that $C_f(t)$ and $C_m(t)$ are the concentration of free and phosphorylated ^{18}F-FDG in the extravascular lung tissue. We would then have the following differential equations to describe the system states:

$$\frac{d}{dt}\begin{bmatrix} C_f(t) \\ C_m(t) \end{bmatrix} = \begin{bmatrix} -k_2 - k_3 & 0 \\ k_3 & 0 \end{bmatrix}\begin{bmatrix} C_f(t) \\ C_m(t) \end{bmatrix} + \begin{bmatrix} K_1 \\ 0 \end{bmatrix} C_p(t), \quad \text{Eq. 1}$$

where K_1 (mL/min/cm^3) and k_2 (/min) indicate the blood-to-tissue and tissue-to-blood ^{18}F-FDG delivery rate constants, respectively. k_3 (/min) is the ^{18}F-FDG phosphorylation rate constant. This irreversible model assumes that the dephosphorylation process is negligible (i.e., the dephosphorylation rate constant $k_4 = 0$) (*13*).

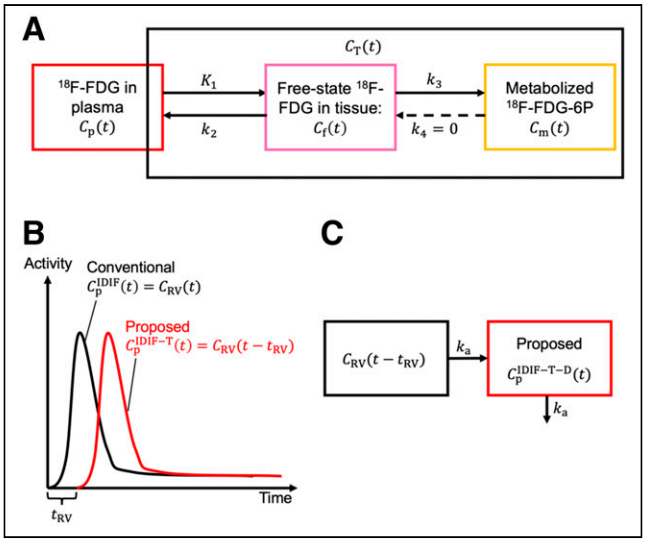

FIGURE 1. (A) Compartmental model of lung kinetics. (B) Proposed IDIF-T model with correction of time delay in input function. (C) Proposed IDIF-T-D model with both time-delay and dispersion corrections included.

The ^{18}F-FDG concentration in lung parenchyma, $C_t(t)$, is the summation of the free and the phosphorylated ^{18}F-FDG,

$$C_t(t) = C_f(t) + C_m(t) = H(t;\boldsymbol{\kappa}) \otimes C_p(t), \quad \text{Eq. 2}$$

where $\boldsymbol{\kappa} = [K_1,\ k_2,\ k_3]^T$, $\otimes$ denotes the convolution operation, and $H(t;\boldsymbol{\kappa})$ is the impulse response function of the 2Ti model:

$$H(t;\boldsymbol{\kappa}) = \frac{K_1}{k_2 + k_3}\left(k_3 + k_2 e^{-(k_2 + k_3)t}\right). \quad \text{Eq. 3}$$

The measured lung time–activity curve obtained by PET is modeled by $C_T(t)$, a mixture of the blood compartment and the tissue compartment,

$$C_T(t) = (1 - v_b)H(t;\boldsymbol{\kappa}) \otimes C_p(t) + v_b C_{wb}(t). \quad \text{Eq. 4}$$

$C_{wb}(t)$ is the whole blood activity and is usually approximated by $C_p(t)$ for ^{18}F-FDG.

Following previous studies (*2,34,35*), the right ventricle IDIF can be used for the blood input,

$$C_p^{IDIF}(t) = C_{RV}(t), \quad \text{Eq. 5}$$

because the pulmonary circulation accounts for most of the total blood input to the lung (*32*).

The measured lung time–activity curve $\check{C}_T(t)$ was fitted with the model time–activity curve $C_T(t)$ using a nonlinear least-squares formulation:

$$\hat{\boldsymbol{\theta}} = \arg\min_{\boldsymbol{\theta}} WRSS(\boldsymbol{\theta}),\ WRSS(\boldsymbol{\theta}) = \sum_{m=1}^{M} w_m[\check{C}_T(t_m) - C_T(t_m)]^2 \quad \text{Eq. 6}$$

where $WRSS(\boldsymbol{\theta})$ denotes the weighted residual sum of squares of the curve fitting. $\boldsymbol{\theta}$ is the unknown parameter set, $\boldsymbol{\theta} = [v_b, K_1,\ k_2,\ k_3]^T$. t_m is the time of the m-th frame in a total of M frames, and w_m is the weight for frame m considering the time length and nuclear decay (*36*):

$$w_m = \Delta t_m \exp(-\lambda t_m). \quad \text{Eq. 7}$$

Here Δt_m is the length of the m-th frame, $\lambda = \frac{\ln(2)}{T_{1/2}}$ is the decay constant, and the half-life $T_{1/2} = 109.8$ min for ^{18}F-FDG. This time-varying weight was based on our initial studies of model fitting.

Modeling of Time-Delay Effect

Corrections for time delay were seldom considered in previous studies of lung kinetic modeling (*2,26–28*) because the delay was usually only several seconds and tended to be blurred out by conventional dynamic imaging of limited temporal resolution (e.g., 10 s/frame). However, the time-delay effect will no longer be concealed with the HTR measurement (e.g., 1 s/frame) and is likely to affect parameter quantification if not accounted for.

To model the time-delay effect of the IDIF extracted from the right ventricle, we include a time-delay parameter t_{RV} (s) in the input function (Fig. 1B):

$$C_p^{IDIF-T}(t) = C_{RV}(t - t_{RV}). \quad \text{Eq. 8}$$

The proposed input function model with time-delay correction is noted as IDIF-T. The time-delay parameter t_{RV} is included in $\boldsymbol{\theta}$ and will be jointly estimated with other kinetic parameters during time–activity curve fitting.

Simultaneous Correction for Dispersion

Dispersion may occur when the tracer travels from the right ventricle to the lung capillaries. Here, we model the actual lung blood input as the convolution of the measured IDIF with a parameterized dispersion function following Iida's monoexponential form (*24,37*),

$$C_{\mathrm{p}}^{\mathrm{IDIF-T-D}}(t) = C_{\mathrm{p}}^{\mathrm{IDIF-T}}(t) \otimes k_{\mathrm{a}}\exp(-k_{\mathrm{a}}t) = C_{\mathrm{RV}}(t-t_{\mathrm{RV}}) \otimes k_{\mathrm{a}}\exp(-k_{\mathrm{a}}t). \quad \text{Eq. 9}$$

This input function model is denoted as IDIF-T-D (Fig. 1C), in which both the dispersion parameter k_{a} (/min) and time delay t_{RV} (s) are included in $\boldsymbol{\theta}$ for joint parameter estimation.

Note that here the simultaneous dispersion correction is different from those explored for brain PET (*25*). Previous work focused on a backward dispersion-correction problem (*24,25*). The measured input function, such as by arterial blood sampling from the radial artery, is a dispersed version of the actual input function. Therefore, the dispersion needs to be removed from the measured input function. In comparison, our work here is a forward dispersion-correction problem. The actual lung input function is a dispersed version of the measured IDIF, to which the dispersion needs to be added.

Evaluation of Time–Activity Curve Fit Quality

The Akaike information criterion (AIC) was used to compare the statistical fit quality of different models (*38,39*),

$$\mathrm{AIC} = M\ln\left(\frac{WRSS}{M}\right) + 2N + \frac{2N^2+2N}{M-N-1}, \quad \text{Eq. 10}$$

where N is the number of unknown parameters to be optimized in $\boldsymbol{\theta}$ and M is the number of dynamic frames. AIC reflects the trade-off between the goodness of fit and the simplicity of the model and thus accounts for the difference in the number of parameters that need to be estimated. A lower AIC value indicates better fitting quality.

Evaluation of the Impact on Kinetic Quantification

We evaluated the impact of the corrections on the quantification of 3 kinetic parameters of interest: ^{18}F-FDG delivery rate K_1, net influx rate K_{i}, and fractional blood volume v_{b}. K_{i} was calculated from the microparameters:

$$K_{\mathrm{i}} = \frac{K_1 k_3}{k_2 + k_3}. \quad \text{Eq. 11}$$

The change in each kinetic parameter by a given model was reported relative to the parameter estimate by the standard IDIF model, and the reason for the quantification changes was studied by analyzing the time–activity curve fittings of different models.

Identifiability Analysis of Kinetic Parameter Estimates

As the proposed models have more parameters to estimate than the standard 2Ti model with the uncorrected IDIF, their kinetic parameter identifiability may be a concern. That is because a more complex model is more likely to be sensitive to random noise and may have reduced parameter stability. To evaluate the parameter identifiability, a noisy lung tissue time–activity curve $\tilde{C}_{\mathrm{T}}(t_m)$ was simulated using a time-varying gaussian model (*40–42*):

$$\tilde{C}_{\mathrm{T}}(t_m) \sim N(\overline{C}_{\mathrm{T},m},\ S_{\mathrm{c}}\delta_m). \quad \text{Eq. 12}$$

where $\overline{C}_{\mathrm{T},m}$ is the m-th frame of the noise-free time–activity curve generated by the curve fitting of the tested model. S_{c} is the scaling factor controlling the noise level and δ_m is the unscaled standard deviation given by:

$$\delta_m = \sqrt{\frac{\overline{C}_{\mathrm{T},m}\exp(\lambda t_m)}{\Delta t_m}} \quad \text{Eq. 13}$$

S_{c} was estimated using the residual error between the measured $\check{C}_{\mathrm{T}}(t)$ and the modeled $C_{\mathrm{T}}(t)$ using the model that demonstrated the best fitting by assuming that the fitting error of that model comes mostly from random noise. We simulated 500 noisy lung tissue time–activity curve realizations for each $\tilde{C}_{\mathrm{T}}(t)$ and analyzed the bias and noise SD of each parameter estimate. The analysis was conducted for the 3 models (i.e., the IDIF, IDIF-T, and IDIF-T-D) using the HTR data. By summing the corresponding HTR frames together, the IDIF model using a more conventional low temporal resolution (10 s/frame in the first 3 min) was also included for comparison.

Correlation of Lung ^{18}F-FDG Kinetics with Age

Aging effects are evident in healthy lungs. Previous human studies have observed an inverse relationship between age and pulmonary blood volume (*43,44*). Therefore, we hypothesize that the v_{b} in the lungs tends to decrease with aging. Although we do not have longitudinal data on individuals in this study, we aim to explore any association between the ^{18}F-FDG kinetic parameters and age using the available healthy subject cohort. We performed the Pearson regression analysis

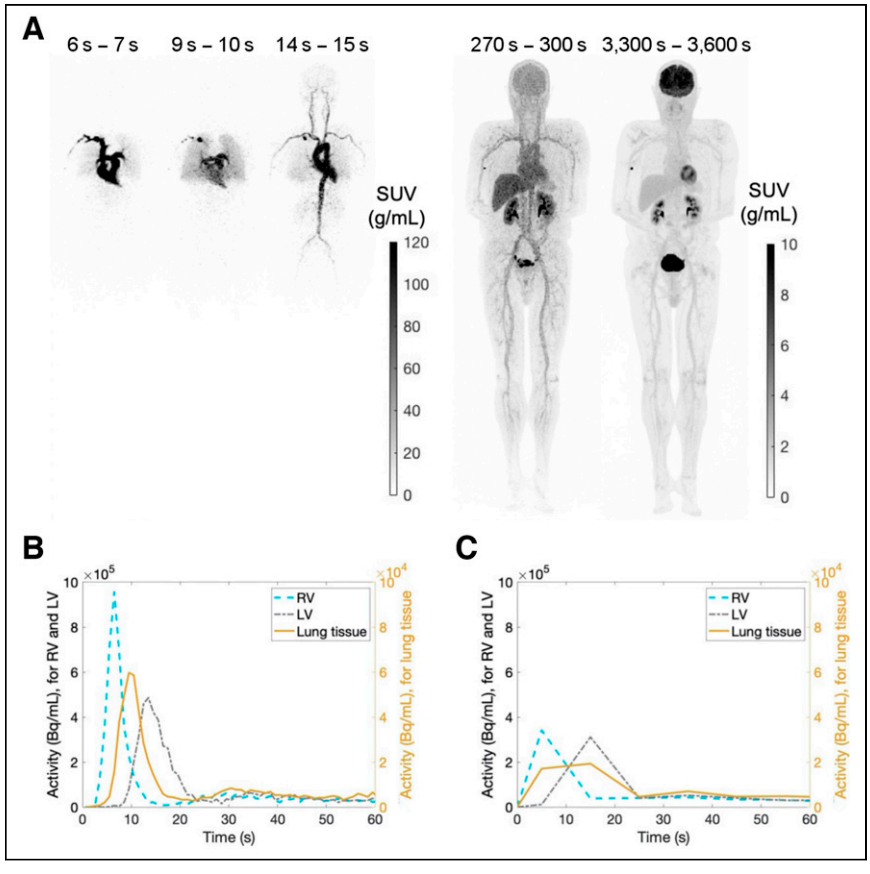

FIGURE 2. (A) HTR (1 s/frame) total-body ^{18}F-FDG dynamic images of example subject acquired using uEXPLORER system. (B) Regional time–activity curves extracted from HTR dynamic images. *y*-axis on left is for time–activity curves of right ventricle and left ventricle, whereas *y*-axis on right is for time–activity curve of lung tissue, which has lower range by factor of 10. (C) Conventional low-temporal-resolution (10 s/frame) regional time–activity curves. LV = left ventricle; RV = right ventricle.

between age and kinetic parameters. Body mass index was also included in the regression to consider potential confounding factors.

Demonstration of Total-Lung Parametric Imaging

In addition to the ROI-based kinetic analysis, we implemented the proposed kinetic modeling approach voxel by voxel. Parametric images of different kinetic parameters (e.g., K_1, K_i, and v_b) were then generated for the entire lung. Kernel smoothing was applied to both the dynamic images and the parametric images for noise reduction (*23*).

RESULTS

Example of HTR Dynamic Images and Time–Activity Curves

Figure 2 shows the acquired HTR total-body dynamic data for a representative subject. The ^{18}F-FDG dynamics in the very early phases after injection were captured by the HTR, as illustrated by the total-body maximum-intensity projections of the SUV image in the coronal direction (Fig. 2A) and the HTR time–activity curves (Fig. 2B). To begin, the tracer was injected into a vein in the right arm before traveling to the right ventricle through the vena cava (Fig. 2A, 6–7 s of the scan time). The tracer next traveled through the pulmonary circulation by flowing into the lungs via the pulmonary artery (Fig. 2A, 9–10 s) and flowing out of the lungs to the left ventricle through the pulmonary veins (Fig. 2A, 14–15 s).

As a comparison, time–activity curves with the conventional temporal resolution are shown in Figure 2C. With a 10-s temporal resolution, the time–activity curves have lost much of the information about the early-phase ^{18}F-FDG kinetics. Both the shape and the amplitude of the time–activity curves were distorted and inaccurate because of the poor temporal resolution.

Model Fitting of Lung Time–Activity Curve

The proposed approaches for modeling the input function can clearly impact the time–activity curve fitting, as shown by the fitting results for an example subject in Figure 3A along with the residual fitting errors in Figure 3B. These figures focus on the early dynamic phase, given that the late phase is similar among different models. Without the time-delay correction, the conventional IDIF model failed to fit the early-phase data even though the time delay is approximately 3 s (Supplemental Fig. 1A; supplemental materials are available at http://jnm.snmjournals.org). The dispersion correction in the IDIF-T-D model further improved the fitting of the first peak because it accounts for the deformation of the input function caused by the tracer dispersion effect (Supplemental Fig. 1B). The improved fitting by the proposed models (IDIF-T and IDIF-T-D) is further demonstrated by the decreased AIC (Fig. 3C; Table 1). The IDIF-T-D model achieved the best average AIC across all subjects.

Kinetic Parameter Estimation

The means and SDs of lung kinetic parameters are reported in Table 2. Figure 4 shows the resulting impact on the quantification of K_1, K_i, and v_b.

When the IDIF model without time-delay or dispersion correction is used, the K_1 value of 0.350 ± 0.092 mL/min/cm^3 seems unreasonable because of the poor fitting. This further supports that the direct application of the IDIF without corrections is not appropriate for the HTR data. The model IDIF-T was also likely to overestimate K_1 given the poor early-phase fitting. The IDIF-T-D estimate of K_1 is 0.056 ± 0.033 mL/min/cm^3, with an approximately 85% decrease compared with the conventional IDIF model. The IDIF-T-D model estimated v_b to be 0.144 ± 0.030, much higher than the estimate obtained with the IDIF (0.042 ± 0.022) and IDIF-T (0.107 ± 0.024) models. A previous study showed a

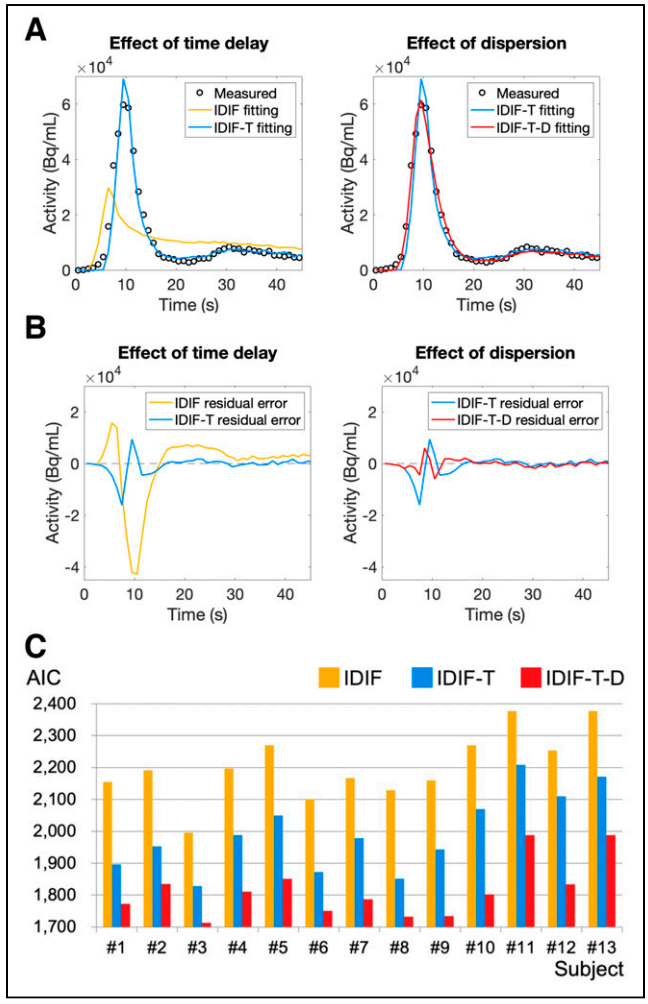

FIGURE 3. (A) Effects of modeling time delay and dispersion on fitting of measured lung time–activity curve. (B) Effects on residual error of time–activity curve fitting. (C) AIC of different models in 13 subjects.

blood fraction of 0.16 in the normal human lungs (*13*). Thus, the v_b estimates by IDIF and IDIF-T are likely biased, whereas the estimates by IDIF-T-D are more consistent with the expected v_b values. For K_i quantification, the proposed IDIF-T-D had an average increase of approximately 75% compared with the conventional IDIF model.

To understand the observed changes in parameter estimation, we analyzed the predicted activity of individual compartments (Supplemental Fig. 2). The vascular component $v_bC_p(t)$ was much increased in the IDIF-T-D model as compared with the IDIF due to the increased v_b estimate. Therefore, the total extravascular component $C_t(t)$ was decreased (Eqs. 2 and 4; Supplemental Fig. 2C), and K_1 became smaller accordingly (Eq. 3). In addition,

TABLE 1
AIC Values of Different Kinetic Models Averaged from 13 Subjects

Model	AIC
IDIF	2,203.2 ± 106.6
IDIF-T	1,993.6 ± 121.3
IDIF-T-D	1,815.2 ± 87.9

TABLE 2
Lung ^{18}F-FDG Kinetic Quantification of K_1, v_b, K_i, t_{RV}, and k_a Using Different Models

Parameter	IDIF	IDIF-T	IDIF-T-D
K_1(mL/min/cm^3)	0.350 ± 0.092	0.190 ± 0.066	0.056 ± 0.033
v_b	0.042 ± 0.022	0.107 ± 0.024	0.144 ± 0.030
K_i(mL/min/cm^3)	0.00034 ± 0.00032	0.00072 ± 0.00039	0.00060 ± 0.00033
t_{RV}(s)	—	3.2 ± 0.5	2.1 ± 0.4
k_a(/min)	—	—	25.8 ± 7.1

K_i was higher in IDIF-T-D than in IDIF because of the increased $C_m(t)$ (Supplemental Fig. 2D), which was associated with decreased K_1 and k_2 but increased k_3.

Identifiability of Kinetic Parameters

Table 3 shows the absolute value of relative bias and the SD of kinetic parameter estimates by different models. To clarify, this analysis is to study the robustness of models against random noise, whereas the systematic bias introduced by model oversimplification (e.g., neglecting the time-delay effect) is not involved. The HTR IDIF model had a lower bias and SD for K_1 and v_b, along with worse K_i estimation, than the low-temporal-resolution IDIF. Among the HTR cases, both the IDIF-T-D and the IDIF models have a small bias (<2%) for K_1 quantification, whereas the SD level of the IDIF-T-D (13.6%) was higher than that of the HTR IDIF (2.4%). The proposed IDIF-T-D model achieved a low bias (<1%) and a low SD (<3%) for quantifying v_b. For K_i, the IDIF-T-D had bias (0.4%) and SD (6.2%) levels comparable to those of the HTR IDIF. The time-delay and dispersion parameters t_{RV} and k_a had good identifiability.

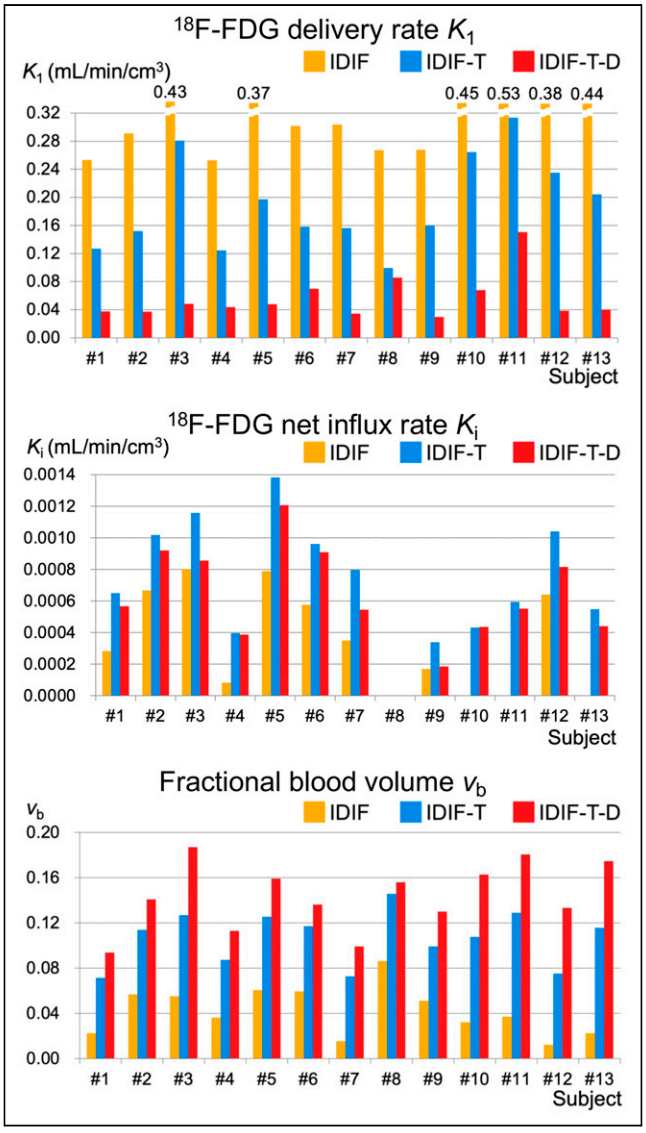

FIGURE 4. Kinetic parameter estimates by different lung kinetic models (IDIF, IDIF-T, and IDIF-T-D).

Correlation with Age

Figure 5 shows the correlation plots between age and v_b estimated by different approaches. For comparison, the result by a traditional low-temporal-resolution protocol (10 s/frame) is also included. Neither the v_b estimates by the low-temporal-resolution approach nor the v_b estimates by the HTR approaches without time-delay or dispersion correction showed a statistically significant correlation with age (all $P > 0.1$). In comparison, the v_b by the proposed IDIF-T-D model correlated with age with statistical significance ($r^2 = 0.45$, $P = 0.01$). The observed age–v_b relationship is consistent with the results reported in previous studies (*43,44*) that show aging to be associated with decreased pulmonary blood volume. Neither age nor body mass index correlated with other kinetic parameters.

Demonstration of Total-Lung Parametric Images

Figure 6A shows the total-lung SUV and multiparametric images using the proposed IDIF-T-D model for a single subject. These images are overlaid on the corresponding CT image. The different parametric images demonstrate complementary spatial information. Figure 6B further shows the parametric images of v_b for a young subject (aged 26 y) and an old subject (aged 78 y). The lung v_b was much lower in this old subject than in the young subject. We also noticed that in the parametric images generated by the IDIF-T-D model, the posterior part of the lungs had a higher v_b than the anterior part, and the posterior lung base had a higher v_b than the apex (Supplemental Fig. 3), which are also within expectation (*45*).

DISCUSSION

In this work, we studied the time-delay and dispersion corrections to the IDIF for lung kinetic modeling with HTR. Traditionally, limited by the temporal resolution of dynamic PET imaging, these corrections were not considered in most existing studies of pulmonary ^{18}F-FDG kinetics (*2,26,46*), especially when the focus

TABLE 3
Relative Bias (Absolute Value) and SD of Kinetic Parameters in Identifiability Study

	IDIF, LTR		IDIF, HTR		IDIF-T, HTR		IDIF-T-D, HTR	
Parameter	Bias (%)	SD (%)	Bias (%)	SD (%)	Bias (%)	SD (%)	Bias (%)	SD (%)
K_1	4.0	9.3	1.3	2.4	6.2	6.4	1.4	13.6
v_b	0.8	6.3	0.5	4.8	1.6	2.7	0.1	2.3
K_i	0.9	4.9	2.4	8.6	4.9	5.4	0.4	6.2
t_{RV}	—	—	—	—	4.5	0.1	0.4	2.8
k_a	—	—	—	—	—	—	1.2	7.2

LTR = low temporal resolution.

was on ^{18}F-FDG K_i (*2,13*), a macroparameter of which the estimation is dominated more by the late-phase dynamic data and is expected to be less sensitive to these corrections. However, a model without these corrections resulted in a poor fitting performance for the HTR data acquired with total-body PET in this work (Figs. 3A and 3C).

The proposed approaches to correcting time delay and dispersion for the IDIF led to much-improved lung time–activity curve fitting (Figs. 3A and 3B) with much lower AIC values (Table 1). Along with the improved fitting, the proposed modeling approaches had a significant impact on kinetic parameter quantification, especially for K_1 and v_b (Table 2). This impact can be explained by the improved estimation of the vascular component in the fitted lung time–activity curves (Supplemental Fig. 2). We also noted that the time delay t_{RV} tended to correlate with the inverse of the dispersion parameter k_a ($r = 0.44$, $P = 0.14$) in the proposed model, as is consistent with the expectation that a longer time delay (larger t_{RV}) is likely to be accompanied by a larger dispersion (smaller k_a). Although the proposed model is more complex, the identifiability analysis results suggested the robustness of the proposed model to random noise (Table 3).

Although there is no ground truth, the v_b estimates by the proposed model are in general more consistent with the literature-reported pulmonary blood volume values and have led to an improved inverse correlation with age (Fig. 5). This correlation aligns with previous findings of decreased pulmonary capillary blood volume with aging (*43,44*). The same correlation would be otherwise missed if the conventional IDIF models with or without time-delay correction were used. Together with the improved time–activity curve fit quality (Fig. 3), our results here indicate the importance of simultaneous time-delay and dispersion corrections as compared with no correction or time-delay correction only (Fig. 5).

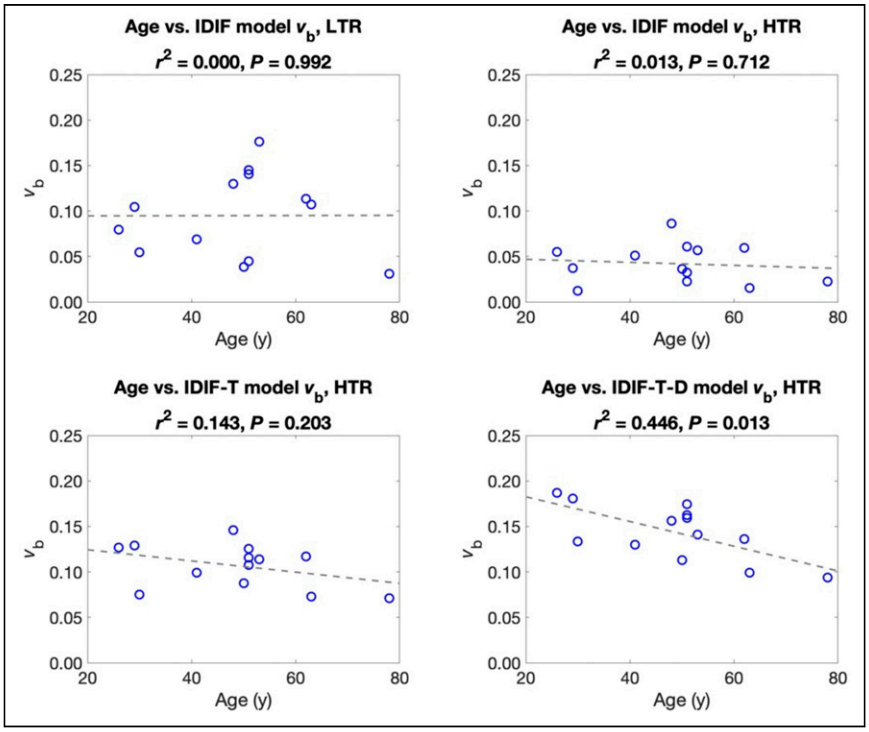

FIGURE 5. Correlation between subject age and v_b using standard IDIF model with 10 s/frame low temporal resolution (top left), IDIF model with 1 s/frame HTR (top right), IDIF-T model with HTR (bottom left), and proposed model IDIF-T-D with HTR (bottom right). LTR = low temporal resolution.

It is worth noting that simultaneous correction for time delay and dispersion was explored previously in dynamic brain PET studies (*25*). However, the method cannot be directly applied in our work on lung kinetic modeling because the prior study tackled a backward dispersion-correction problem that removes dispersion from the measured input function (e.g., from the radial artery), whereas this paper focuses on a forward dispersion-correction problem that adds dispersion to the measured IDIF for modeling the actual blood input. The latter approach is developed in response to the availability of IDIF in total-body HTR dynamic PET imaging.

In addition to the use of the right ventricle for deriving the IDIF, the region of the pulmonary arteries may be used directly for their closer location to the lung tissues. Similar results were obtained using the pulmonary arteries as the input function compared with using the right ventricle, including the input function after corrections (Supplemental Fig. 4A), lung time–activity curve fitting (Supplemental Fig. 4B), and kinetic parameter quantification (Supplemental Table 1),

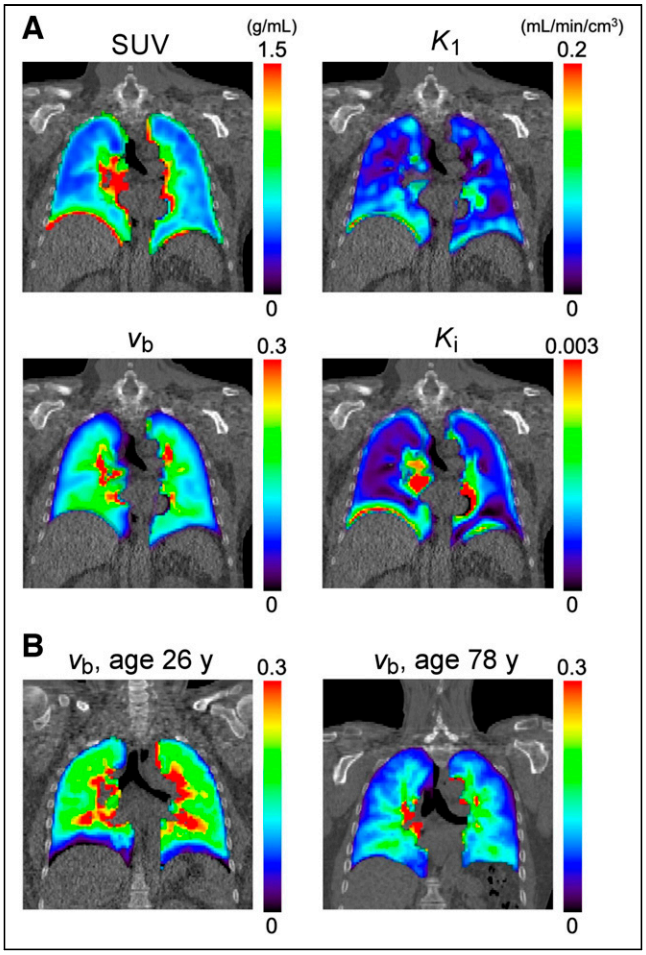

FIGURE 6. (A) ^{18}F-FDG PET images of segmented lung for example subject (subject 4): SUV image of 55–60 min, and multiparametric images of ^{18}F-FDG delivery rate K_1, fractional blood volume v_b, and net influx rate K_i generated with IDIF-T-D model. These images are superimposed on corresponding CT images. (B) v_b images of young subject (subject 3) and old subject (subject 1).

confirming the benefits of time-delay and dispersion corrections. The IDIFs from the left and right pulmonary arteries can also be used for kinetic modeling of individual lungs (Supplemental Table 1). However, use of the pulmonary arteries for IDIF needs to be done more carefully because the smaller size may make ROI placement more challenging to reduce the partial-volume effect.

This work has several limitations. First, the sample size is relatively small as the 13 healthy subjects vary in age and body weight. Second, subject motion can affect the kinetic quantification results (*47*). We tried to minimize the motion effect by carefully placing the ventricular ROIs to reduce the partial-volume effect of the myocardium. We also drew 5 ROIs in the lung lobes and extracted the global lung time–activity curve to decrease the respiratory motion effect and avoid a partial-volume effect from the liver. Third, the air fraction in the lungs may affect the absolute quantification of K_1 and K_i (*27,48*), but the correction is not included here. It does not, however, influence the comparison of kinetic models because this tissue-fraction effect introduces only a scaling factor on K_1 and K_i and can be corrected after kinetic modeling.

Our future work will include a larger subject cohort and apply the method to study lung diseases, such as coronavirus disease 2019. The kinetic quantification approach can be also used to assess the lungs in other systemic diseases, for example, cancer and nonalcoholic fatty liver disease. Motion correction and air fraction correction will be implemented to optimize the HTR kinetic modeling and parameter estimation further. Another direction is to model the dual blood-input function to account for the fraction of tracer delivery from the bronchial circulation (*49*). This dual-input effect may be small in healthy lung tissues but can be significant in lung tumors (*50*), which will be explored in a future study.

CONCLUSION

We studied lung kinetic modeling for HTR dynamic PET imaging on the uEXPLORER total-body PET/CT system. Direct application of the standard IDIF model resulted in poor time–activity curve fitting. We developed an approach to jointly correcting the effects of time delay and dispersion in the IDIF. The proposed model greatly improved time–activity curve fitting and had a large impact on lung kinetic quantification. It also improved the correlation of v_b with age. Total-body HTR dynamic PET has the potential to be a sensitive tool for studying healthy lungs and lung diseases.

DISCLOSURE

This research is supported in part by National Institutes of Health grants R01 CA206187 and R01 DK124803. The University of California at Davis has a research agreement and revenue-sharing agreement with United Imaging Healthcare. No other potential conflict of interest relevant to this article was reported.

ACKNOWLEDGMENTS

We gratefully acknowledge the technologists and staff of the University of California, Davis, EXPLORER Molecular Imaging Center for acquiring and processing the data.

KEY POINTS

QUESTION: Is simultaneous correction of time delay and dispersion essential for high-temporal resolution kinetic modeling of the lungs in total-body dynamic PET imaging?

PERTINENT FINDINGS: The proposed time-delay and dispersion corrections can largely improve model fitting and have a significant impact on lung kinetic quantification, leading to an improved correlation between age and fractional blood volume v_b.

IMPLICATIONS FOR PATIENT CARE: Total-body dynamic PET with HTR kinetic modeling may offer a sensitive tool to evaluate the lungs in health and disease.

REFERENCES

1. Dimitrakopoulou-Strauss A, Hoffmann M, Bergner R, et al. Prediction of short-term survival in patients with advanced nonsmall cell lung cancer following chemotherapy based on 2-deoxy-2-[F-18]fluoro-D-glucose-positron emission tomography: a feasibility study. *Mol Imaging Biol.* 2007;9:308–317.
2. de Prost N, Tucci MR, Melo MFV. Assessment of lung inflammation with ^{18}F-FDG PET during acute lung injury. *AJR.* 2010;195:292–300.
3. Rodrigues RS, Miller PR, Bozza FA, et al. FDG-PET in patients at risk for acute respiratory distress syndrome: a preliminary report. *Intensive Care Med.* 2008;34:2273–2278.
4. Castro M, Fain SB, Hoffman EA, Gierada DS, Erzurum SC, Wenzel S. Lung imaging in asthmatic patients: the picture is clearer. *J Allergy Clin Immunol.* 2011;128:467–478.

5. Chen DL, Schiebler ML, Goo JM, van Beek EJR. PET imaging approaches for inflammatory lung diseases: current concepts and future directions. *Eur J Radiol.* 2017;86:371–376.
6. Fields BKK, Demirjian NL, Dadgar H, Gholamrezanezhad A. Imaging of COVID-19: CT, MRI, and PET. *Semin Nucl Med.* 2021;51:312–320.
7. van den Hoff J, Oehme L, Schramm G, et al. The PET-derived tumor-to-blood standard uptake ratio (SUR) is superior to tumor SUV as a surrogate parameter of the metabolic rate of FDG. *EJNMMI Res.* 2013;3:77.
8. Hellwig D, Graeter TP, Ukena D, et al. ^{18}F-FDG PET for mediastinal staging of lung cancer: which SUV threshold makes sense? *J Nucl Med.* 2007;48:1761–1766.
9. Carson RE. Tracer kinetic modeling in PET. In: *Positron Emission Tomography.* Springer; 2005:127–159.
10. Mullani NA, Herbst RS, O'Neil RG, Gould KL, Barron BJ, Abbruzzese JL. Tumor blood flow measured by PET dynamic imaging of first-pass ^{18}F-FDG uptake: a comparison with ^{15}O-labeled water-measured blood flow. *J Nucl Med.* 2008;49:517–523.
11. Laffon E, Calcagni ML, Galli G, et al. Comparison of three-parameter kinetic model analysis to standard Patlak's analysis in ^{18}F-FDG PET imaging of lung cancer patients. *EJNMMI Res.* 2018;8:24.
12. de Prost N, Feng Y, Wellman T, et al. ^{18}F-FDG kinetics parameters depend on the mechanism of injury in early experimental acute respiratory distress syndrome. *J Nucl Med.* 2014;55:1871–1877.
13. Chen DL, Cheriyan J, Chilvers ER, et al. Quantification of lung PET images: challenges and opportunities. *J Nucl Med.* 2017;58:201–207.
14. Chen DL, Schuster DP. Positron emission tomography with [^{18}F]fluorodeoxyglucose to evaluate neutrophil kinetics during acute lung injury. *Am J Physiol Lung Cell Mol Physiol.* 2004;286:L834–L840.
15. Wellman TJ, de Prost N, Tucci M, et al. Lung metabolic activation as an early biomarker of acute respiratory distress syndrome and local gene expression heterogeneity. *Anesthesiology.* 2016;125:992–1004.
16. Dimitrakopoulou-Strauss A, Georgoulias V, Eisenhut M, et al. Quantitative assessment of SSTR2 expression in patients with non-small cell lung cancer using ^{68}Ga-DOTA-TOC PET and comparison with ^{18}F-FDG PET. *Eur J Nucl Med Mol Imaging.* 2006;33:823–830.
17. Cherry SR, Badawi RD, Karp JS, Moses WW, Price P, Jones T. Total-body imaging: transforming the role of positron emission tomography. *Sci Transl Med.* 2017;9:eaaf6169.
18. Surti S, Pantel AR, Karp JS. Total body PET: Why, how, what for? *IEEE Trans Radiat Plasma Med Sci.* 2020;4:283–292.
19. Nadig V, Herrmann K, Mottaghy FM, Schulz V. Hybrid total-body pet scanners: current status and future perspectives. *Eur J Nucl Med Mol Imaging.* 2022;49:445–459.
20. Zhang X, Cherry SR, Xie Z, Shi H, Badawi RD, Qi J. Subsecond total-body imaging using ultrasensitive positron emission tomography. *Proc Natl Acad Sci USA.* 2020;117:2265–2267.
21. Feng T, Zhao Y, Shi H, et al. Total-body quantitative parametric imaging of early kinetics of ^{18}F-FDG. *J Nucl Med.* 2021;62:738–744.
22. Li EJ, Spencer BA, Schmall JP, et al. Efficient delay correction for total-body PET kinetic modeling using pulse timing methods. *J Nucl Med.* 2022;63:1266–1273.
23. Wang G, Nardo L, Parikh M, et al. Total-body PET multiparametric imaging of cancer using a voxel-wise strategy of compartmental modeling. *J Nucl Med.* 2022;63:1274–1281.
24. Iida H, Kanno I, Miura S, Murakami M, Takahashi K, Uemura K. Error analysis of a quantitative cerebral blood flow measurement using $H_2{}^{15}O$ autoradiography and positron emission tomography, with respect to the dispersion of the input function. *J Cereb Blood Flow Metab.* 1986;6:536–545.
25. Meyer E. Simultaneous correction for tracer arrival delay and dispersion in CBF measurements by the $H_2{}^{15}O$ autoradiographic method and dynamic PET. *J Nucl Med.* 1989;30:1069–1078.
26. Chen DL, Mintun MA, Schuster DP. Comparison of methods to quantitate ^{18}F-FDG uptake with PET during experimental acute lung injury. *J Nucl Med.* 2004;45:1583–1590.
27. Holman BF, Cuplov V, Millner L, et al. Improved correction for the tissue fraction effect in lung PET/CT imaging. *Phys Med Biol.* 2015;60:7387–7402.
28. Schroeder T, Vidal Melo MF, Musch G, Harris RS, Venegas JG, Winkler T. Modeling pulmonary kinetics of 2-deoxy-2-[^{18}F]fluoro-D-glucose during acute lung injury. *Acad Radiol.* 2008;15:763–775.
29. Spencer BA, Berg E, Schmall JP, et al. Performance evaluation of the uEXPLORER total-body PET/CT scanner based on NEMA NU 2-2018 with additional tests to characterize PET scanners with a long axial field of view. *J Nucl Med.* 2021;62:861–870.
30. Leung EK, Berg E, Omidvari N, et al. Quantitative accuracy in total-body imaging using the uEXPLORER PET/CT scanner. *Phys Med Biol.* 2021;66:205008.
31. West JB. Evolution of the pulmonary circulation and the right heart. In: *Pulmonary Circulation.* CRC Press; 2016:22–30.
32. Walker CM, Rosado-de-Christenson ML, Martínez-Jiménez S, Kunin JR, Wible BC. Bronchial arteries: anatomy, function, hypertrophy, and anomalies. *Radiographics.* 2015;35:32–49.
33. Cherry SR, Sorenson JA, Phelps ME. Tracer kinetic modeling. In: *Physics in Nuclear Medicine.* 4th ed. Elsevier Health Sciences; 2012:379–405.
34. de Prost N, Costa EL, Wellman T, et al. Effects of surfactant depletion on regional pulmonary metabolic activity during mechanical ventilation. *J Appl Physiol.* 2011;111:1249–1258.
35. Schroeder T, Vidal Melo MF, Musch G, Harris RS, Venegas JG, Winkler T. Image-derived input function for assessment of ^{18}F-FDG uptake by the inflamed lung. *J Nucl Med.* 2007;48:1889–1896.
36. Thiele F, Buchert R. Evaluation of non-uniform weighting in non-linear regression for pharmacokinetic neuroreceptor modelling. *Nucl Med Commun.* 2008;29:179–188.
37. Wang G, Corwin MT, Olson KA, Badawi RD, Sarkar S. Dynamic PET of human liver inflammation: impact of kinetic modeling with optimization-derived dual-blood input function. *Phys Med Biol.* 2018;63:155004.
38. Akaike H. A new look at the statistical model identification. *IEEE Trans Automat Contr.* 1974;19:716–723.
39. Glatting G, Kletting P, Reske SN, Hohl K, Ring C. Choosing the optimal fit function: comparison of the Akaike information criterion and the F-test. *Med Phys.* 2007;34:4285–4292.
40. Carson RE, Yan Y, Daube-Witherspoon ME, Freedman N, Bacharach SL, Herscovitch P. An approximation formula for the variance of PET region-of-interest values. *IEEE Trans Med Imaging.* 1993;12:240–250.
41. Wu Y, Carson RE. Noise reduction in the simplified reference tissue model for neuroreceptor functional imaging. *J Cereb Blood Flow Metab.* 2002;22:1440–1452.
42. Zuo Y, Sarkar S, Corwin MT, Olson K, Badawi RD, Wang G. Structural and practical identifiability of dual-input kinetic modeling in dynamic PET of liver inflammation. *Phys Med Biol.* 2019;64:175023.
43. Georges R, Saumon G, Loiseau A. The relationship of age to pulmonary membrane conductance and capillary blood volume. *Am Rev Respir Dis.* 1978;117:1069–1078.
44. Chang S-C, Chang H-I, Liu S-Y, Shiao G-M, Perng R-P. Effects of body position and age on membrane diffusing capacity and pulmonary capillary blood volume. *Chest.* 1992;102:139–142.
45. Galvin I, Drummond GB, Nirmalan M. Distribution of blood flow and ventilation in the lung: gravity is not the only factor. *Br J Anaesth.* 2007;98:420–428.
46. Grecchi E, Veronese M, Moresco RM, et al. Quantification of dynamic [^{18}F]FDG PET studies in acute lung injury. *Mol Imaging Biol.* 2016;18:143–152.
47. Hunter CRRN, Klein R, Beanlands RS, deKemp RA. Patient motion effects on the quantification of regional myocardial blood flow with dynamic PET imaging. *Med Phys.* 2016;43:1829–1840.
48. Coello C, Fisk M, Mohan D, et al. Quantitative analysis of dynamic ^{18}F-FDG PET/CT for measurement of lung inflammation. *EJNMMI Res.* 2017;7:47.
49. Deffebach ME, Charan NB, Lakshminarayan S, Butler J. The bronchial circulation. *Am Rev Respir Dis.* 1987;135:463–481.
50. Yuan X, Zhang J, Ao G, Quan C, Tian Y, Li H. Lung cancer perfusion: can we measure pulmonary and bronchial circulation simultaneously? *Eur Radiol.* 2012;22:1665–1671.